

A Comparative Evaluation of NOAA/AVHRR Vegetation Indexes for Burned Surface Detection and Mapping

José M. C. Pereira

Abstract—The only vegetation index (VI) used in all Advanced Very High Resolution Radiometer (AVHRR)-based burned area studies performed so far is the normalized difference vegetation index (NDVI), in spite of serious known deficiencies caused by sensitivity to atmospheric conditions and soil background. In this study, the ability of various VI to discriminate between burned and unburned surfaces is compared, using burn maps derived from classification of Landsat thematic mapper (TM) imagery as reference data. After assessing the discriminatory potential of the AVHRR channels 1–3, the following indexes were compared: the NDVI, the VI 3 (VI3), the global environmental monitoring index (GEMI), and a modified version of GEMI, called GEMI3. VI performance was assessed in two ways: with a signal-to-noise ratio measure and a measure of the commission error resulting from segmentation of the burned area histograms at a fixed level of omission error. Maps of commission errors were generated for each VI and cross tabulated with a land cover map to identify the land cover types more prone to confusion with burns. The newly proposed index GEMI3 performs best, followed by the GEMI, VI3, and finally NDVI, the latter being clearly out performed, even by channel 2 used individually.

Index Terms— Burned areas, discrimination, mapping, NOAA/Advanced Very High Resolution Radiometer (AVHRR), vegetation indexes.

I. INTRODUCTION

WILDFIRES in southern Europe burn hundreds of thousands of hectares of forests, shrub lands, and grasslands every year, causing extensive economical and ecological losses and, often, human casualties. The fire season throughout most of Portugal, Spain, France, Italy, and Greece occurs during the period of June–September, corresponding to the warm to hot and dry summer, typical of Mediterranean climates. Analyses of fire size statistics [1], [2] reveal a pattern of great concentration of the total area burned in a relatively small number of large fires, similar to those found for Southern California and Northern Baja California [3], [4] and for Canada [5]. This pattern suggests that it may be viable to use coarse spatial resolution imagery, such as that provided by the NOAA Advanced Very High Resolution Radiometer (AVHRR) to detect and map a large proportion of the area annually burned in this region [6], [7]. An additional advantage

of such an approach would be the production of timely and methodologically consistent burned area statistics for the whole region.

Spectral vegetation indexes (VI's) derived from satellite imagery provide a simple and fast method to map vegetation abundance and have previously been used for burned area detection and mapping using the AVHRR [6]–[12] and the Landsat thematic mapper (TM) [13]–[20]. The only VI used in all of the above-mentioned AVHRR-based studies was the normalized difference vegetation index (NDVI), developed in the early 1970's [21] and extensively used ever since, in spite of serious deficiencies caused by sensitivity to atmospheric and soil background effects [22]–[24]. Therefore, in this study, the capacity of various VI to discriminate between burned and unburned surfaces is compared analyzing a single date subscene over a study area located in central Portugal, using burned area maps derived from classification of Landsat TM imagery as the reference, because a semiempirical analysis of the latter is believed to yield an accurate description of the spatial distribution of burned areas. The purpose is not to suggest VI image analysis as a sufficient methodology for burned area mapping, but to compare the relative performance of different VI, assuming that those which perform best on a single date will also be the most adequate for multitemporal studies, and for inclusion in more complex, multiple thresholding procedures.

II. STUDY AREA AND DATA

The region selected for our analysis (Fig. 1) exhibits intense fire activity. The study region (28 710 km²) was chosen as the area covered by Landsat 5 TM scenes 203/32 and 204/32, centered at 40.33° N, 6.93° W and 40.33° N, 8.50° W, respectively. During the 1980–1989 period, in the most severely burned counties of this region, an area approximately equivalent to 75% of the total county area was affected by fire [25]. The study area has diverse landscapes and three main topographic regions: the westernmost section is a coastal plain, densely populated, mainly agricultural, with scattered maritime pine (*Pinus pinaster*) and mixed (mostly *P. pinaster* and *Eucalyptus globulus*) forests, forming a fragmented landscape, not prone to large fires; the central part is more mountainous and densely covered by the same forest types, replaced in some areas by relatively extensive shrublands that often represent various stages of postfire succession, this area is especially

Manuscript received October 9, 1996; revised November 14, 1997. This work was supported by the MEGAFIRES Project (Contract ENV4-CT96-0256), funded by DGXII of the European Commission.

The author is with the Departamento de Engenharia Florestal, Instituto Superior de Agronomia, 1300 Lisbon, Portugal.

Publisher Item Identifier S 0196-2892(99)00037-6.

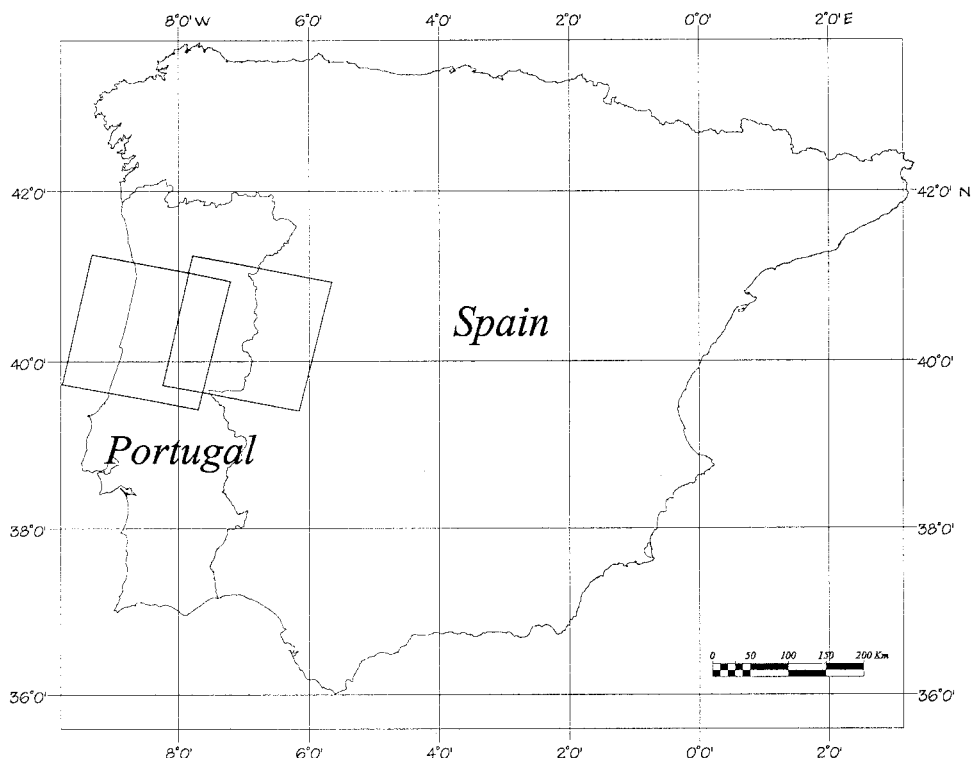


Fig. 1. Study area location.

prone to large fires; and the eastern part of the region is a relatively sparsely populated plateau, where extensive dry-land farming of cereal crops is the dominant agricultural land use, interspersed with shrublands and evergreen oak (*Quercus sp.*) woodlands. Elevation ranges from sealevel at the western edge of the study area (i.e., the Atlantic coast) to 2000 m slightly to the east of the center of the area.

Two TM images dated 11.8.1991 (203/32) and 2.3.1992 (204/32) were used to provide validation data for the analysis performed on an NOAA-11 AVHRR high-resolution picture transmission (HRPT) image acquired on September 16, 1991, at 14:44 h, under a near-nadir observation geometry. The 1991 fire season was the worst on record in Portugal, with over 180 000 ha burned, and almost all of this area had burned previous to the date of acquisition of the AVHRR image. Thus, the age of burned surfaces visible in the scene ranges from a few days up to four months.

III. METHODS

A. Image Preprocessing and Generation of a Fire Mask

The AVHRR image was navigated and calibrated to top-of-the-atmosphere (TOA) reflectances (channels 1 and 2) and brightness temperatures (channels 3–5, including nonlinearity corrections), using the software package developed at the Colorado Center for Astroynamics Research [28], [29]. The image was then geometrically corrected with ground control points digitized from 1:250 000 scale maps and referenced to the Gauss–Kruger map projection with nearest neighbor resampling. The root mean square error (RMSE) of this procedure was smaller than one AVHRR pixel. Very simple

water and cloud masks were applied: the Atlantic Ocean, to the west of the study area boundary, was masked out using a coastline map digitized from 1:250 000 scale maps, and a coastal cloud bank was removed with a manually digitized mask.

The two Landsat TM scenes were also geometrically corrected and resampled to the same map projection using ground control points obtained from 1:25 000 scale maps, to an accuracy of better than one TM pixel, and then mosaicked side-by-side. The TM data were not calibrated, and the classification of burned surfaces was performed on the raw digital counts with a parallelepiped classifier, using channels 2–7. Channel 1 was avoided due to excessive atmospheric contamination.

Classification of burned surfaces with the Landsat TM images for construction of the spatial mask was performed in three steps. First, a conservative classification was performed, using narrow thresholds in the parallelepiped classifier to avoid commission errors. Then, spatial buffers up to a distance of 700 m (deemed adequate by visual inspection of the images) were automatically drawn around the areas classified as burned, and finally, a second, less restrictive parallelepiped classification was performed, affecting only the inside of these buffers. It was found that this methodology effectively eliminated much of the confusion between burned surfaces and other sparsely vegetated areas, which had been previously identified as problematic in burned area detection and mapping [16]. The use of a spatial adjacency constraint to classify less thoroughly burned areas has also been reported [7], [12] and seems quite appropriate and effective, considering that burns are, in most cases, generated by a spatial diffusion process. Results of the supervised classification process were compared

with field-drawn fire perimeters for 60 fires obtained by the Instituto Florestal, of the Portuguese Ministry of Agriculture, and found to be very accurate [30]. Nonetheless, the vector files resulting from the TM image classification were overlaid on a 743 red–green–blue color composite image and edited manually, when necessary. For the purposes of the present study, all burns with an area smaller than 120 ha (one AVHRR pixel) were discarded.

B. Refinement of the Burned Area Mask

After having obtained an image representing the reflectance in channel 3, a 321 red–green–blue color composite was generated using the TOA reflectances of the three AVHRR. The vector file containing the high-resolution fire perimeters obtained through classification of the TM data was overlaid on this AVHRR color composite, and it was found that there was a spatial mismatch of about one AVHRR pixel in a diagonal NW–SE direction. The high-resolution mask was linearly shifted 1555 m toward the SE, clearly improving coregistration between the two data layers. The high-resolution burned area mask was then degraded to the AVHRR pixel resolution to segment the three AVHRR channels into burned and unburned classes. However, due to some residual spatial mismatch and omission and commission errors caused by the spatial degradation process, it was decided to use the degraded burned area mask vector file, together with its high-resolution counterpart, to redigitize the fire boundaries on screen, over the AVHRR color composite. This helped minimize the spatial degradation and misregistration problems that would arise from direct application of the TM-derived mask to segment the AVHRR image. The procedure employed still made full use of the TM classification results, both at the original 30-m resolution and at the degraded 1100-m resolution, assisting in the visual delineation of the fire boundaries on the AVHRR image. It is considered that this procedure did not bias the detection of burned areas in favor of any specific index since the spectral information contained in the three channels was used simultaneously.

C. Single-Channel Analysis and Selection of Vegetation Indexes

Prior to the selection of VI for the study, an analysis of the potential of AVHRR red, near infrared (NIR), and MIR channels for burned area detection and mapping was performed (following a suggestion by M. Verstraete and B. Pinty). Although the majority of AVHRR-based burned area detection and mapping studies have used data from the red and NIR spectral ranges, several studies using Landsat TM indicate the potential usefulness of the MIR range [14], [15], [17], [19], [20]. Channel 3 data were evaluated under two formats: using the full radiance of the surface (i.e., the sum of the emitted and reflected components of the signal) and only the reflected component. Channel 3 reflectance was determined following the procedure outlined by [31] and [32].

Based on results of this analysis, a set of four VI were selected: the NDVI [21] and the global environmental monitoring index (GEMI) [33], defined in the red-NIR bispectral

space, and the VI3 [32], and the GEMI3, a modified GEMI introduced in this study (suggested by B. Pinty and M. Verstraete), both defined in the NIR-MIR bispectral space. Although the assessment of individual channel performance indicated that the AVHRR channel 1 has the least discriminant power of all channels tested, it was decided to evaluate VI defined in the red-NIR spectral space because most of the available knowledge concerning the spectral properties of earth surface features refers to this domain. Also, the AVHRR channels 1 and 2, although lacking onboard calibration and subject to temporal drifting of the calibration coefficients, are not affected by the various noise problems from which channel 3 has suffered [34], [35]. The NDVI was chosen because it is one of the oldest, certainly the most widely used VI in a great variety of terrestrial vegetation studies [36] and recently selected as the VI for inclusion in the IGBP global 1-km resolution data set [37].

The GEMI was selected as representative of a new generation of improved vegetation indexes, specifically designed to minimize problems of contamination of the vegetation signal by extraneous factors, such as the atmosphere and the soil background. Its nonlinear design provides a significant built-in attenuation of atmospheric effects [33], considered very important for the remote sensing of dark surfaces, such as recently burned areas. The GEMI has also been shown to be functionally unrelated to the NDVI [24] and, at least under some circumstances, better than the NDVI for assessing fractional vegetation cover [23].

The NIR–MIR bispectral space is considered attractive for burned surface detection and mapping, despite the potential channel 3 noise problems mentioned above, for two main reasons. First, the 3.5–4- μm region of AVHRR channel 3 overlaps with a water absorption band and is thus very sensitive to the presence of liquid water. Burned surfaces, which are partially or totally devoid of green vegetation, and present very dry soil surfaces especially shortly after the fire, therefore, appear quite bright in this spectral range and contrast strongly with the very low reflectance displayed in the NIR. Second, replacing channel 1 by channel 3 results in a considerable reduction of sensitivity to the atmosphere, especially, but not exclusively to, the effect of atmospheric aerosols. Since smoke and haze layers are often present in imagery of burned surfaces, this is a particularly desirable feature of the NIR–MIR spectral domain. The VI3 was designed as a normalized difference index based on these concepts, and performance for the detection of dense dark vegetation has been compared to that of the NDVI [32].

GEMI3 is proposed as an empirical modification of the GEMI since the values of the coefficients in the GEMI formula, which were kept unchanged, are not expected to retain their original physical interpretation. However, this decision was based on the fact that the range of reflectance values over the study area was similar for channels 1 and 3. Also, it was expected that the nonlinear behavior that makes the GEMI an effective cloud detector [26], due to the high reflectance of clouds in channel 1, would perform likewise for burns, which were the most reflective surfaces in channel 3 after cloud-screening of the study area. Therefore, GEMI3 was meant to explore the synergistic effects of the desirable spectral

properties of the AVHRR channel 3 reflective component, with the more sophisticated nonlinear design of the GEMI. Under these circumstances, merits of the GEMI3 will be assessed only on practical, empirical grounds.

The equations for the four VI selected, using the AVHRR, are the following:

$$\text{NDVI} = (\rho_2 - \rho_1) / (\rho_2 + \rho_1) \quad (1)$$

$$\text{VI3} = (\rho_2 - \rho_3) / (\rho_2 + \rho_3), \quad \text{for } \rho_2 \geq \rho_1$$

or

$$\text{VI3} = 0, \quad \text{for } \rho_2 < \rho_1 \quad (2)$$

$$\text{GEMI} = \eta(1 - 0.25\eta) - (\rho_1 - 0.125) / (1 - \rho_1) \quad (3)$$

where

$$\eta = (2(\rho_2^2 - \rho_1^2) + 1.5\rho_2 + 0.5\rho_1) / (\rho_2 + \rho_1 + 0.5). \quad (4)$$

For the GEMI3, ρ_3 takes the place of ρ_1 in (3) and (4).

Each symbol represents the following:

ρ_1 TOA reflectance in channel 1 (0.58–0.68 μm);

ρ_2 TOA reflectance in channel 2 (0.725–1.1 μm);

ρ_3 TOA reflectance in channel 3 (3.55–3.93 μm).

D. Assessment of Single-Channel and VI Burned Area Discrimination Ability

Visual inspection of a grayscale or color-coded image containing burned surfaces is not an adequate methodology for assessing the discriminant capability of spectral indexes. It is necessary to quantify this ability, taking into account both the magnitude of interclass differences as well as the magnitude of intraclass variance, for some predefined set of land cover classes. In this study, it was decided to consider only two classes, one formed by surfaces burned during the 1991 fire season and another containing all remaining land cover types. Since the study area under analysis is quite diverse, this approach imposes a considerable degree of potential intraclass variability, at least on the generic background class, and thus represent a very stringent test for the ability of VI to detect and characterize burned areas. On the other hand, it should guarantee that results are more reliable than if a very detailed, site-specific land cover classification had been used.

The measure used to quantify the effectiveness of each spectral channel and vegetation index to separate burned surfaces from the unburned background environment is given by [32]

$$M = (\mu_u - \mu_b) / (\sigma_u + \sigma_b) \quad (8)$$

where

μ_u mean value for the unburned background class;

μ_b mean value for the burned area class;

σ_u standard deviation of values for the unburned background class;

σ_b standard deviation of values for the burned area class.

Values of M larger than one indicate good separability, while values smaller than one represent a large degree of histogram overlap between the two classes. This measure is

analogous to the signal-to-noise ratio concept previously used to evaluate the performance of various VI as predictors of fractional vegetation cover [23] and to the ratios of between-group variance to within-group variance used in ANOVA and discriminant analysis. Here, the difference between mean values of the two classes represents the burned area detection signal, or between-group variance, while the sum of the standard deviations measures the level of noise, or within-group variance, confounding discrimination of the two classes. The use of statistical tests of hypotheses, such as Student's t-test or Kolmogorov–Smirnov's test as spectral separability measures, was judged inadequate since the study area is considered as a population of pixels and not a sample of a broader region. The appropriate statistical techniques are descriptive, not inferential. Even if the study area were to be taken as a sample, application of conventional techniques of statistical inference would be problematic since the high-spatial autocorrelation inherent in the data would artificially inflate significance levels. Use of a correct statistical procedure, such as a spatial two-way ANOVA [38], is precluded by the large size of the data set [39].

An additional indication of VI performance was derived to provide information on the spatial extent, distribution, and qualitative nature of commission errors in burned area classification once a given level of omission error is prespecified. Since the VI minima for all indexes are obtained inside burned areas, partially as a result of the water and cloud masking performed on the AVHRR imagery, burned/unburned image segmentations were set at the eighty-fifth, ninetieth, and ninety-fifth percentile of the burned class histogram. These levels of, respectively, 15, 10, and 5% omission error were considered as representing an error range for burned area quantification, acceptable for most applications in regional or global studies. All pixels below these levels were classified as burned, and all pixels above were classified as unburned. The burned areas mask was then used to eliminate the correctly classified burned pixels, leaving only a burned class commission error mask. These masks were overlaid on a land cover map to determine the land cover types more prone to be confused with burned surfaces by the various VI's.

IV. RESULTS

A. Spectral Discrimination Index M

Figs. 2 and 3 show the histograms of the burned and unburned classes, which are useful in understanding the behavior of each VI for burned area detection and mapping. The distances between the mean values for the two classes, the amount of spread in the data, and the consequent extent of histogram overlap determine the values of the spectral discrimination index M . Fig. 2 clearly shows that channel 2 ($M = 1.05$) and the reflective component of channel 3 ($M = 0.62$) separate better the two classes, while in channel 1 ($M = 0.36$) and in channel 3 normalized total radiance ($M = 0.60$) the degree of overlap is higher. The figure also shows that burned surfaces tend to be darker than the background environment in channels 1 and 2, but brighter in

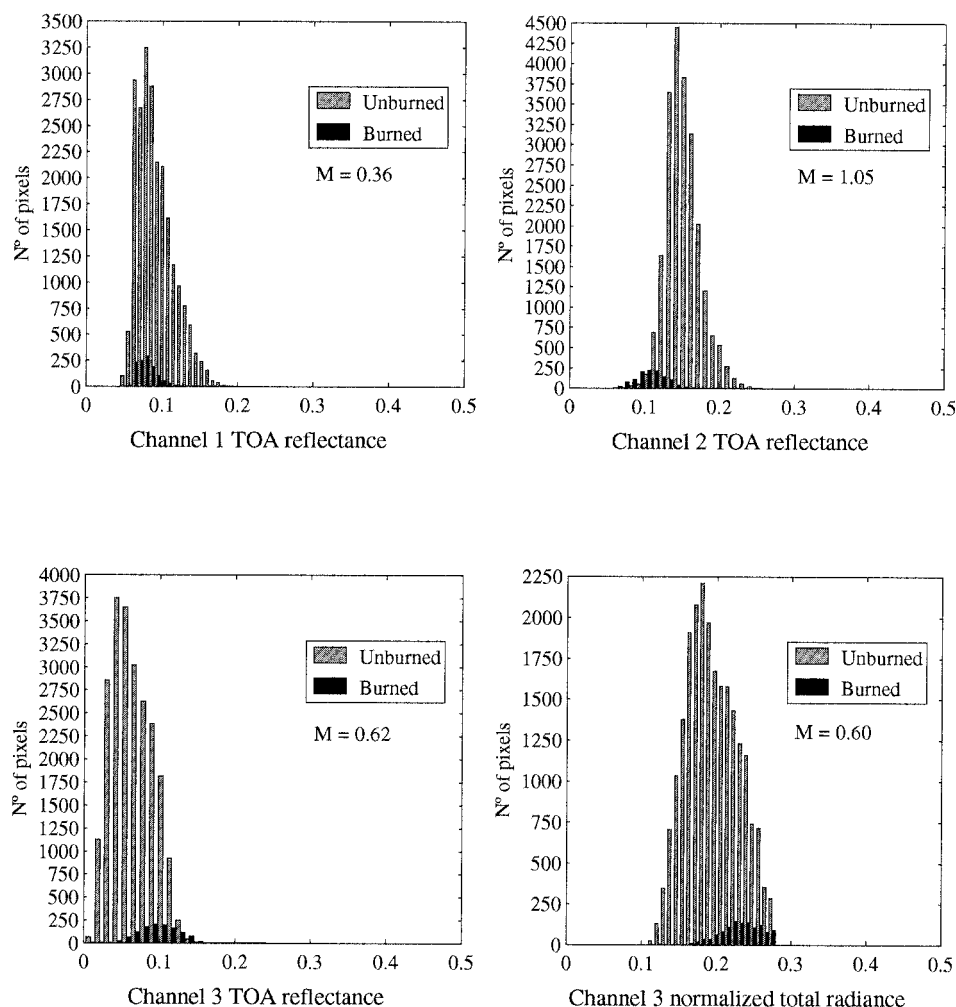


Fig. 2. Histograms of the burned and unburned classes for the four individual NOAA/AVHRR channels evaluated.

channel 3. Based on these results, it was decided to use the reflective component of channel 3 for the vegetation indexes defined in the NIR–MIR bispectral space and further evaluate the burned area mapping potential of channel 2 with the commission error assessment procedure.

Fig. 3 presents results for the four VI. The GEMI3 displays the largest discriminant power ($M = 1.38$), followed by the GEMI and VI3, with similar scores ($M = 1.19$ and $M = 1.15$). However, this similarity of scores hides clearly different behaviors, as illustrated by the histograms. While the GEMI discriminates well between the two classes, essentially due to the very small within-group variance, since the means are not widely separated, the VI3 is able to separate the means broadly, but this is more than offset by a very large within-group variance. The GEMI3 performs better than both by exhibiting an intermediate behavior. Relative to the VI3, it clearly loses a large amount of signal (i.e., between-group variance), but makes up for this by a drastic reduction in the level of within-group variance. In comparison with the GEMI, there are gains in signal detection and losses in noise-reduction ability, but also with a positive net outcome. The NDVI ($M = 0.75$) is the worst of the four VI tested and clearly worse than channel 2 used individually.

B. Commission Errors for a Fixed Level of Omission Error

Table I shows the magnitude of the commission error for the eighty-fifth, ninetieth, and ninety-fifth percentile thresholdings of the burned area histogram and the breakdown of these errors by land cover type. The magnitude and spatial distribution of the commission errors for each index, when an omission error of 10% is set for the burned class, are shown in Fig. 4.

The NDVI commission error was quite extensive (46.5% of the study area) and concentrated on the eastern half of the study area. The VI3 error (17.8%) was also concentrated in the same region, but it covered a smaller area and showed a more fragmented pattern. VI3 performs very well in the westernmost region, where few fires occurred. Channel 2 (17.5% total commission error) displays a very different spatial pattern of commission error from the previous two indexes. It performed much better than both the NDVI and VI3 in the eastern third of the study area, but worse than both in the central part and worse than the VI3 in the western coastal plain. The spatial extent of the commission error was obviously smaller for the GEMI (12.5%), and concentrated in the central and eastern regions. Finally, the GEMI3 performed best (total commission error of 5.7%), with a very scattered error pattern, and two

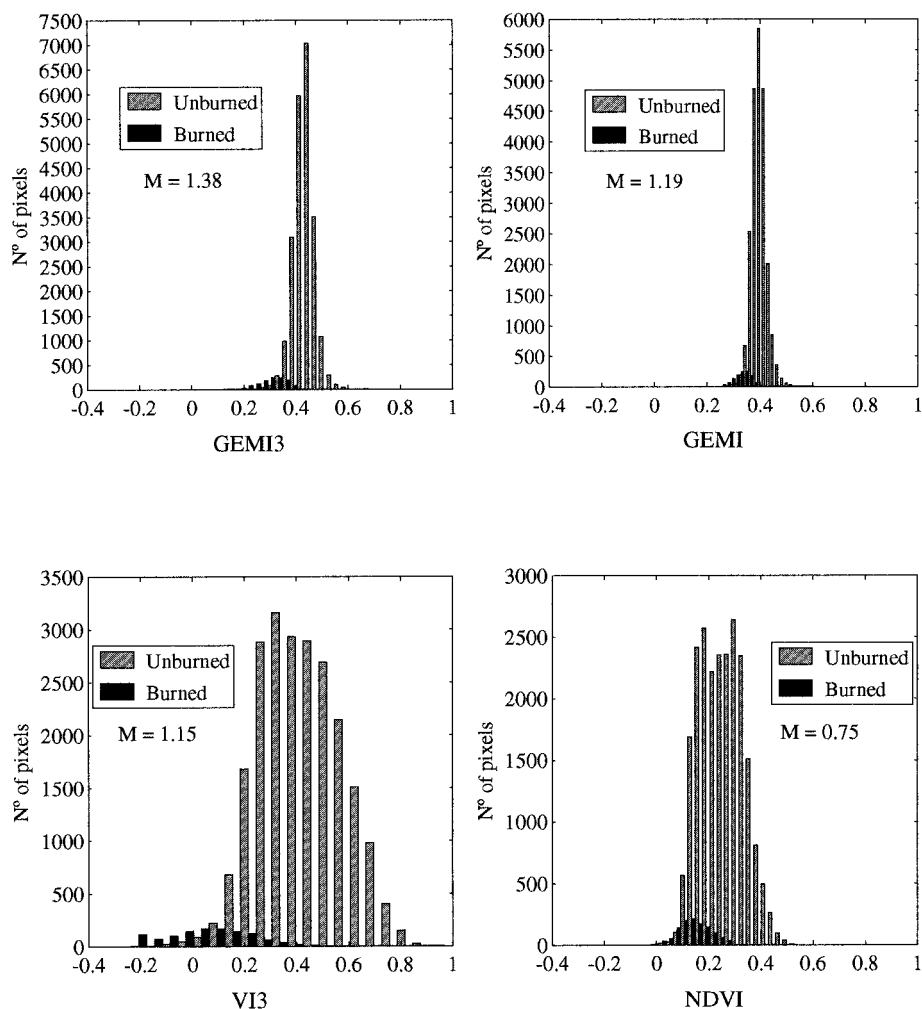


Fig. 3. Histograms of the burned and unburned classes for the four NOAA/AVHRR-based vegetation indexes evaluated.

regions of almost perfect performance, along the west coast and in the southeastern corner of the study area.

Results of the breakdown of commission error by land cover type for each VI and level of omission error are presented in Table I, as proportions of area misclassified as burned relative to the total area of each land cover type. This normalization of the data was considered useful since it highlights the performance of each index for each land cover type, neutralizing the effect of land cover type abundance in the study area. The very poor performance of the NDVI in the eastern region is associated with lower vegetation densities and "greenness" levels, especially at the end of what was a very warm and dry summer. The NDVI extensively misclassifies as burns areas of evergreen oak woodlands (the hardwoods class), agricultural fields with cereal stubble, and a mixed land use class, where cereal crops are grown in the understory of sparse oak woodlands (the agroforestry land cover type). Urban areas and grasslands are also prone to confusion with burns by the NDVI, which performs relatively better with the coniferous and the mixed forest types.

The AVHRR channel 2, on the contrary, performs best at discriminating burns, very dark in the NIR, from the bright surfaces that dominate the landscape of eastern Portugal at

the end of the summer. The land cover types more prone to confusion with burned surfaces in the NIR are the conifer and mixed forest and, to a lesser extent, barren ground, wetlands, and water, the areas classified in the CORINE land cover map as having burned during 1985 and 1986. The confusion with barren ground is the hardest to interpret since all other land cover types tend to be dark in the NIR.

The distribution of VI3 commission errors by land cover type was similar to that of the NDVI, but it covered a much smaller area. Higher proportions of misclassified pixels occurred in association with high albedo land cover types, but this index is very good at discriminating burns from wetlands and water.

The GEMI performed quite well overall, but especially over the agricultural and sparse evergreen oak landscapes of eastern Portugal. It displayed slightly higher error levels over the conifer and mixed forests, shrub lands, old burns, and barren ground. The highest proportions of GEMI commission errors occurred with wetlands and water. The GEMI3 was clearly the best of all indexes tested for the purpose of segmenting images into burned and unburned areas. It performed well over the drier landscapes of eastern Portugal and on barren ground, made slightly higher commission errors over the forest, shrub

TABLE I

PROPORTIONS OF BURNED AREA CLASSIFICATION COMMISSION ERROR, AT 15% (FIRST ROW), 10% (SECOND ROW), AND 5% (THIRD ROW) OMISSION ERROR LEVELS, FOR EACH LAND COVER TYPE. PROPORTIONS HIGHER THAN 0.2 ARE GRAY-SHADED, TO HIGHLIGHT THE MOST PROBLEMATIC LAND COVER TYPES FOR EACH SPECTRAL DISCRIMINATOR

| Land cover type | GEMI3 | GEMI | VI3 | Ch2 | NDVI |
|-----------------|-------|-------|-------|-------|-------|
| urban | 0.020 | 0.110 | 0.020 | 0.100 | 0.510 |
| | 0.020 | 0.140 | 0.140 | 0.120 | 0.580 |
| | 0.060 | 0.230 | 0.240 | 0.210 | 0.790 |
| agriculture | 0.029 | 0.063 | 0.100 | 0.076 | 0.499 |
| | 0.042 | 0.105 | 0.196 | 0.098 | 0.560 |
| | 0.075 | 0.201 | 0.399 | 0.210 | 0.667 |
| grassland | 0.000 | 0.071 | 0.095 | 0.024 | 0.548 |
| | 0.000 | 0.095 | 0.214 | 0.048 | 0.643 |
| | 0.071 | 0.167 | 0.500 | 0.095 | 0.786 |
| agro-forestry | 0.000 | 0.016 | 0.046 | 0.007 | 0.664 |
| | 0.000 | 0.036 | 0.237 | 0.007 | 0.720 |
| | 0.003 | 0.118 | 0.513 | 0.007 | 0.763 |
| hardwood | 0.029 | 0.042 | 0.090 | 0.037 | 0.541 |
| | 0.040 | 0.073 | 0.215 | 0.045 | 0.627 |
| | 0.064 | 0.139 | 0.440 | 0.111 | 0.735 |
| conifers | 0.044 | 0.086 | 0.061 | 0.363 | 0.205 |
| | 0.065 | 0.146 | 0.102 | 0.416 | 0.272 |
| | 0.118 | 0.274 | 0.203 | 0.736 | 0.432 |
| mixed forest | 0.054 | 0.099 | 0.073 | 0.328 | 0.212 |
| | 0.077 | 0.146 | 0.110 | 0.379 | 0.288 |
| | 0.121 | 0.236 | 0.232 | 0.750 | 0.426 |
| shrublands | 0.049 | 0.085 | 0.119 | 0.120 | 0.393 |
| | 0.068 | 0.140 | 0.201 | 0.141 | 0.446 |
| | 0.116 | 0.252 | 0.355 | 0.255 | 0.527 |
| old burns | 0.053 | 0.107 | 0.101 | 0.218 | 0.274 |
| | 0.090 | 0.169 | 0.163 | 0.249 | 0.329 |
| | 0.158 | 0.274 | 0.274 | 0.417 | 0.433 |
| barren ground | 0.016 | 0.129 | 0.097 | 0.242 | 0.323 |
| | 0.016 | 0.145 | 0.177 | 0.258 | 0.403 |
| | 0.032 | 0.306 | 0.306 | 0.419 | 0.661 |
| wetlands | 0.087 | 0.283 | 0.000 | 0.250 | 0.315 |
| | 0.152 | 0.283 | 0.000 | 0.250 | 0.315 |
| | 0.217 | 0.283 | 0.022 | 0.272 | 0.337 |
| water | 0.107 | 0.192 | 0.073 | 0.205 | 0.303 |
| | 0.141 | 0.209 | 0.107 | 0.218 | 0.325 |
| | 0.184 | 0.252 | 0.205 | 0.286 | 0.368 |

land, and old burn land cover types, and like the GEMI, it performed poorest over wetlands and water. This should be considered a minor problem since these land cover types tend to be quite stable and well known and, thus, can be masked out of a scene quite easily.

V. DISCUSSION

A. Areas Burned During the Previous Year

There was substantial agreement between the two quantitative criteria selected to assess VI capacity to discriminate burned areas from a diverse and complex environmental background. Both the M measure and the magnitude of commission error for the three omission error levels identify the GEMI3 as the best spectral discriminator, with the GEMI, VI3, and channel 2 ranked in intermediate positions, and the NDVI in last place. This ordinal ranking of VI performance is probably more robust than the precise quantitative values of M and percent of commission errors, mainly because of two aspects of the performance assessment procedure. First,

burned areas from the previous year (1990) were allocated to the unburned background class in the segmentation performed with the 1991 burned area mask, partly because TM-derived fire perimeters for 1990 were unavailable. However, these areas still display spectral characteristics similar to those of the recent (i.e., 1991) burns and, therefore, contribute to an artificial increase of the spectral variability of the unburned background class. But since they had already lost most of the charcoal residue left by the fire, and vegetation recovery had started, their inclusion in the burned category could have extended the right-side tail of the histogram for this category and increased the overlap with the unburned class (Figs. 2 and 3). Visual observation of the VI images and inspection of the reflectance values over areas known to be one year-old burns suggest that the reported values of M and the magnitude of commission errors possibly underestimate true VI discriminant ability. Some amount of error is also inevitably associated with the estimates of the extent to which each land cover type was misclassified as burned because of land cover changes during the 1986–1991 period. However, these changes are known to have affected a sufficiently small part of the study area, such that the results presented ought to be valid.

B. Interpretation of VI Behavior

The various VI tested confused burns with diverse types of surfaces. The NDVI and VI3 predominantly misclassified as burned surfaces the land cover types of the drier part of the study area. At the end of the summer, dry crop residues, senesced grasslands, and relatively bright bare soils are abundant in this region. These surfaces have high reflectance, both in the red and NIR, resulting in NDVI values close to zero and prone to confusion with the recent burns, which are quite dark in both spectral regions. The relatively higher albedo land cover types of eastern Portugal in the late summer also produce VI3 values close to zero, due to high reflectance in the 3.75- μm region. However, confusion with burns is less of a problem because thoroughly burned areas display high MIR reflectance, resulting in negative values of the VI3. Problems remain for moderately brighter surfaces in which $\rho_3 > \rho_2$, such as in partially burned areas.

The VI3 is quite effective at discriminating burned surfaces from wetlands and lakes because, even though these land cover types tend to be mixtures of water with vegetation and/or soils, they are darker in the AVHRR channel 3 than in channel 1. This is due to the sensitivity of the 3.75- μm region to liquid water in vegetation and the virtual absence of an aerosol-induced atmospheric effect in this spectral region. On the contrary, burned areas, especially at the end of a Mediterranean-type summer, are usually very dry surfaces, and this is likely to be the cause for their relatively high reflectance in the MIR. Therefore, VI3 mixed pixels with spectral signatures dominated by the presence of water have positive values, in the same range as vegetated surfaces, while burns typically present negative values. The channel 2, GEMI, and GEMI3 are more susceptible to misclassify dense forests, wetlands, and water bodies as burned areas, an error pattern also present in the NDVI. Wetlands are ecologically and

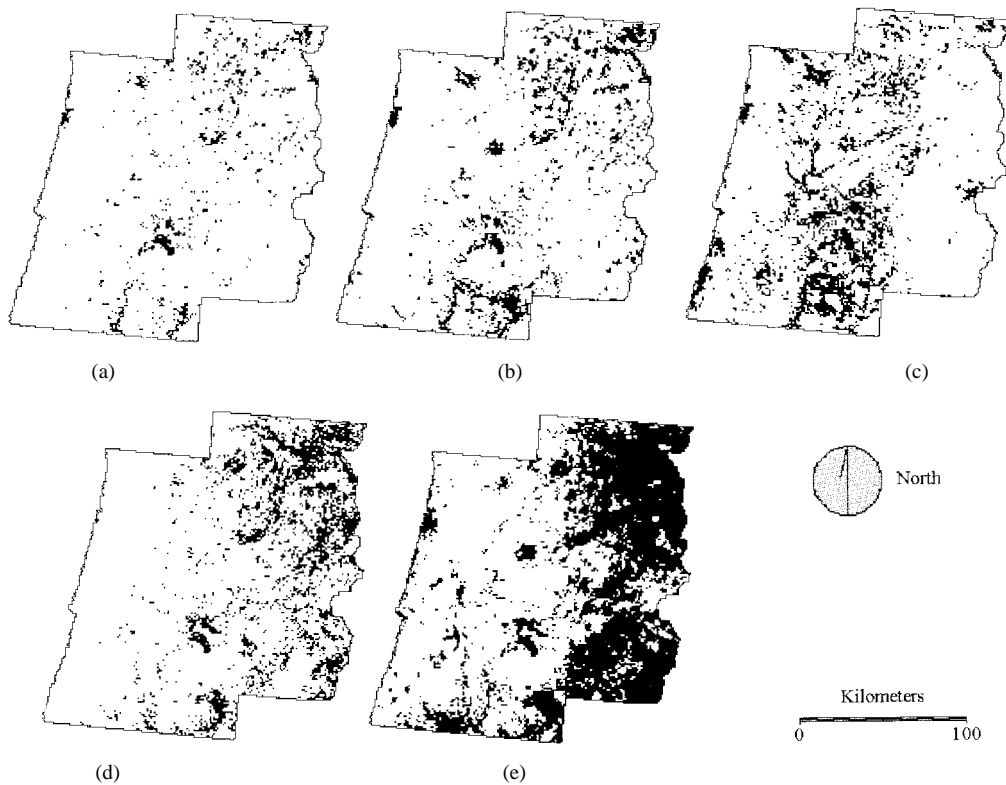


Fig. 4. Maps of commission error in burned area classification for a fixed 10% level of omission error for five indexes: (a) GEMI3, (b) GEMI, (c) Channel 2 TOA reflectance, (d) VI3, and (e) NDVI.

spectrally complex mixtures of water, vegetation, and soils, and the inland water bodies observed in the AVHRR scene also appear as spectral mixtures, essentially due to their relatively small size and the coarse spatial resolution of the sensor. Both land cover types display spectral signatures dominated by water, i.e., with low reflectance in the red, NIR, and MIR. The conifer and mixed forests display typical signatures of relatively dense dark vegetation, with lower NIR reflectance than areas of irrigated agriculture. Therefore, in the NIR range of channel 2 reflectance, many of these surfaces overlap the values found in burned areas.

The same pattern is observed with the NDVI, which displays relatively low positive values over the forests, and values very close to zero over the mixed pixels of the water and wetland classes, a range of NDVI values that is also found in burns. The fact that channel 2 taken individually outperforms the NDVI in burned surface detection seems to suggest that the contribution of channel 1 may be detrimental for burned area mapping, and this is apparently confirmed by the very low M -value obtained for channel 1. A likely explanation for this result is that many dark land cover types, such as water bodies, wetlands, most vegetation types, burned surfaces, and some soil types, show low TOA reflectance in channel 1, and a part of this reflectance is due to atmospheric effects. By comparison, in channel 2, most vegetation types are more reflective and therefore unlikely to be confused with burned surfaces. In channel 3, which is scarcely affected by the atmosphere, vegetation and water are very dark, but on the contrary, burned areas are some of the brightest surfaces observed [17], [20]. Thus, the potential for confusion between

recent burns and other land cover types is highest in the AVHRR visible channel.

The GEMI represents a significant improvement over the NDVI mostly due to the nonlinear response to red and NIR reflectance values. The nonlinear behavior of the GEMI implies that moderately bright to very bright soils (or other types of surfaces located close to the 1:1 line in a red-NIR bispectral space, i.e., senesced herbaceous vegetation) have lower GEMI values than dark surfaces located at a similar distance to the 1:1 line, such as dark soils, water, and wetlands. Considering the narrow dynamic range of the GEMI over the study area (Fig. 2), even small differences may be big enough to eliminate a large amount of confusion between burned surfaces and brighter surfaces close to the 1:1 line in red-NIR spectral space. This interpretation is backed by the observation of an overall decrease in mean albedo values of the commission error areas for the GEMI, relative to the NDVI, where albedo is defined as the arithmetic mean of reflectance values in AVHRR channels 1 and 2 [40].

However, the relatively reduced sensitivity of the GEMI to small variations in surface brightness over dark surfaces [23] implies that some level of confusion between the dark burns and land cover types, such as wetlands and water bodies, still remains. This problem is attenuated by using the MIR channel instead of the red channel, in GEMI3, due to the migration toward lower values of reflectance of areas containing high amounts of water, and toward higher reflectance values of the burned areas. The latter aspect may be either a consequence of the burned surface becoming very dry or result from the spectral properties of combustion products deposited at the soil

surface. Therefore, GEMI3 values for burns drop, while those of other dark surfaces rise, and detectability of burned surfaces is increased with the results shown in Fig. 4 and Table I.

The MIR range may prove to be even more important than in the present study, if burned surfaces have to be detected through smoky or hazy atmospheric conditions, since smoke from biomass burning causes little attenuation of MIR radiation at wavelengths longer than $1.5 \mu\text{m}$ [41]. The good performance of the reflective component of AVHRR channel 3 was confirmed recently with AVHRR imagery from the Central African Republic, gathered during the early dry season of 1996–1997 [42]. A modified NDVI, where the channel 7 of Landsat TM is used, instead of the conventional channel 3, has also been used successfully for burned area mapping in Portugal [20], [30].

VI. CONCLUSIONS

It was shown that, at least for the types of land cover dominant in Mediterranean-type regions, the NDVI is not a good index to detect and map burned surfaces, and better alternatives are available, namely, using channel 2 alone. The largest improvement in ability to detect recent burns with AVHRR imagery was obtained with GEMI3, a modified GEMI, in which the reflective component of AVHRR channel 3 takes the place of channel 1. The nonlinear nature of the GEMI, combined with the sensitivity of the MIR spectral range to soil and plant moisture, were hypothesized as explanations for the behavior of GEMI3. Most of the confusion problems remaining in GEMI3 ought to be relatively simple to solve, either by using static masks for permanent surface features, such as wetlands and inland water bodies, or with multitemporal approaches.

Important topics for further research include verification of the hypothesis that surface dryness is indeed responsible for the high MIR reflectance of burned areas, or whether it is just a consequence of the spectral properties of combustion residues, and multitemporal analyzes, required to perform the following:

- 1) test the hypothesis which states that the VI that performs best on a single postfire season date is also the most accurate for prefire season/postfire season change detection;
- 2) assess accuracy levels of an operational procedure for burn area mapping based on change detection;
- 3) analyze adequate compositing strategies for the detection and analysis of nonvegetated surfaces;
- 4) evaluate the changes in VI performance as a function of burn age.

In relation with accuracy assessment of burned area estimates derived from AVHRR, the TM imagery used for constructing the high-resolution burn mask can be used for this purpose and to develop calibration equations to improve the accuracy of burned area estimation, which has been done quite successfully for forest area estimation [43], [44].

ACKNOWLEDGMENT

The author wishes to thank the Instituto Florestal (IF) and the Centro Nacional de Informação Geográfica (CNIG)

for access to their joint Landsat TM image archive and for construction of the high-resolution burned area map. Dr. J.-P. Malingreau, leader of the MTV Unit, SAI/JRC, Ispra, Italy, provided the pleasant and productive working environment where the final stages of this project were performed. The author also gratefully acknowledges the many instructive and stimulating talks with MTV personnel, namely, M. Verstraete, B. Pinty, and J.-M. Grégoire. The author also thanks Dr. P. Teillet, Canadian Centre for Remote Sensing, for having provided the AVHRR channel 3 exoatmospheric irradiance data. T. Oliveira and J. Paúl (CNIG) preprocessed the AVHRR image and programmed the algorithm for splitting the AVHRR channel 3 radiance. L. Cadete (CNIG) prepared the low-resolution CORINE land cover data. A. Sousa and J. Silva (DEF/ISA) performed the TM image interpretation for the high-resolution burned area map.

REFERENCES

- [1] M. Neves, J. M. C. Pereira, and R. M. Natário, "A statistical analysis of wildfire size data," in *Proc. 2nd Int. Conf. Forest Fires Res.*, Coimbra, Portugal, 1994.
- [2] A. Vázquez and J. M. Moreno, "Patterns of fire occurrence across a climatic gradient and its relationship to meteorological variables in Spain," in *Global Change and Mediterranean-Type Ecosystems*, J. M. Moreno and W. C. Oechel, Eds. Berlin, Germany: Springer-Verlag, Ecological Studies 117, 1995, pp. 408–434.
- [3] R. A. Minnich, "Fire measures in Southern California and Northern Baja California," *Science*, vol. 219, pp. 1287–1294, 1983.
- [4] D. Strauss, L. Bednar, and R. Mees, "Do one percent of forest fires cause ninety-nine percent of the damage," *Forest Sci.*, vol. 35, pp. 319–328, 1989.
- [5] B. J. Stocks, "The extent and impact of forest fires in northern circumpolar countries," in *Global Biomass Burning. Atmospheric, Climatic and Biospheric Implications*, J. S. Levine, Ed. Cambridge, MA: MIT Press, 1991, pp. 197–202.
- [6] J. M. C. Pereira, L. Cadete, and M. J. P. Vasconcelos, "An assessment of the potential of NOAA/AVHRR HRPT imagery for burned area mapping in Portugal," in *Proc. 2nd Int. Conf. Forest Fire Res.*, Coimbra, Portugal, 1994.
- [7] M. Caetano, L. Mertes, L. Cadete, and J. M. C. Pereira, "Assessment of AVHRR data for characterising burned areas and post-fire vegetation recovery," *EARSEL Advances in Remote Sensing*, vol. 4, pp. 124–134, 1996.
- [8] P. Frederiksen, S. Langaas, and M. Mbaye, "NOAA-AVHRR and GIS-based monitoring of fire activity in Senegal—A provisional methodology and potential applications," *Fire in the Tropical Biota. Ecosystem Processes and Global Challenges*, J. G. Goldammer, Ed. Berlin, Germany: Springer-Verlag, Ecological Studies 84, 1990, pp. 400–417.
- [9] J. P. Malingreau, "The contribution of remote sensing to the global monitoring of fires in tropical and subtropical ecosystems," in *Fire in the Tropical Biota, Ecosystem Processes and Global Challenges*, J. G. Goldammer, Ed. Berlin, Germany: Springer-Verlag, Ecological Studies 84, 1990, pp. 333–370.
- [10] E. S. Kasischke, N. H. F. French, P. Harrel, N. L. Christensen, Jr., S. L. Ustin, and D. Barry, "Monitoring wildfires in boreal forests using large area AVHRR NDVI composite image data," *Remote Sens. Environ.*, vol. 45, pp. 61–71, 1993.
- [11] M. P. Martín and E. Chuvieco, "Mapping and evaluation of burned land from multitemporal analysis of AVHRR NDVI images," in *Proc. Int. Workshop Satellite Technol. GIS Mediterranean Forest Mapping Fire Manage.*, P. J. Kennedy and M. Karteris, Eds. EUR 15861 EN, 1993, pp. 71–83.
- [12] E. S. Kasischke and N. H. F. French, "Locating and estimating the areal extent of wildfires in Alaskan boreal forests using multiple-season AVHRR NDVI composite data," *Remote Sens. Environ.*, vol. 51, pp. 263–275, 1995.
- [13] S. Tanaka, H. Kimura, and Y. Suga, "Preparation of a 1 : 25000 Landsat map for assessment of burnt area on Etajima Island," *Int. J. Remote Sensing*, vol. 4, pp. 17–31, 1983.
- [14] A. K. Milne, "The use of remote sensing in mapping and monitoring vegetational change associated with bushfire events in eastern Aus-

- tralia," *Geocarto Int.*, vol. 1, pp. 25–34, 1986.
- [15] F. J. Ponzoni, D. C. L. Lee, and P. H. Filho, "Avaliação da área queimada e da regeneração da vegetação afetada pelo fogo no Parque Nacional de Brasília através de dados do TM/Landsat," in *Proc. Latin-Amer. Remote Sensing Symp., IV Brazilian Remote Sensing Symp.*, 1986, pp. 615–621.
- [16] E. Chuvieco and R. G. Congalton, "Mapping and inventory of forest fires from digital processing of TM data," *Geocarto Int.*, vol. 4, pp. 41–53, 1988.
- [17] M. J. López and V. Caselles, "Mapping burns and natural reforestation using thematic mapper data," *Geocarto Int.*, vol. 1, pp. 31–37, 1991.
- [18] J. M. C. Pereira, "Burned area mapping with conventional and selective principal component analysis," *Finisterra*, vol. 27, pp. 61–76, 1992.
- [19] J. M. C. Pereira and A. W. Setzer, "Spectral characteristics of fire scars in Landsat-5 TM images of Amazonia," *Int. J. Remote Sensing*, vol. 14, pp. 2061–2078, 1993.
- [20] J. M. N. Silva, "Comparação entre os índices de vegetação NDVI e IV7 para cartografia de áreas ardidas com imagens Landsat-5 TM," ISA/UTL, Project Rep., 1996.
- [21] D. W. Deering, J. W. Rouse, R. H. Haas, and J. A. Schell, "Measuring forage production of grazing units from Landsat MSS data," in *Proc. 10th Int. Symp. Remote Sensing Environ.*, 1975, vol. 2, pp. 1169–1178.
- [22] A. R. Huete, "A soil adjusted vegetation index (SAVI)," *Remote Sens. Environ.*, vol. 25, pp. 295–309, 1988.
- [23] C. Leprieur, M. M. Verstraete, and B. Pinty, "Evaluation of the performance of various vegetation indices to retrieve vegetation cover from AVHRR data," *Remote Sens. Rev.*, vol. 10, pp. 265–284, 1994.
- [24] S. Flasse and M. M. Verstraete, "Monitoring the environment with vegetation indices: Comparison of NDVI and GEMI using AVHRR data over Africa," in *Vegetation, Modeling and Climatic Change*, F. Veroustraete and R. Ceulemans, Eds. The Hague, The Netherlands: SPB, 1994, pp. 107–135.
- [25] J. M. C. Pereira, J. M. B. Carreiras, and M. J. P. Vasconcelos, "Exploratory data analysis of the spatial distribution of wildfires in Portugal, 1980–1989," *Geograph. Syst.*, to be published.
- [26] D. Briggs and H. Mounsey, "Integrating land resource data into a European geographical information system: Practicalities and problems," *Appl. Geography*, vol. 9, pp. 5–20, 1989.
- [27] J. C. Wiggins, R. P. Hartley, M. J. Higgins, and R. J. Whittaker, "Computing aspects of a large geographic information system for the European community," *Int. J. Geograph. Inf. Syst.*, vol. 1, pp. 77–87, 1987.
- [28] D. G. Baldwin and W. J. Emery, "A systematized approach to AVHRR image navigation," *Ann. Glaciol.*, vol. 17, pp. 414–420, 1993.
- [29] G. W. Rosborough, D. G. Baldwin, and W. J. Emery, "Precise AVHRR image navigation," *IEEE Trans. Geosci. Remote Sensing*, vol. 32, pp. 644–657, May 1994.
- [30] A. Sousa, J. M. N. Silva, M. E. C. Ziebell, and J. M. C. Pereira, "Cartografia das áreas ardidas em Portugal, para os anos de 1993 e 1994 com imagens do satélite Landsat5 TM," *LDRAG, DEF/ISA*, 1996.
- [31] B. N. Holben and Y. E. Shimabukuro, "Linear mixing model applied to coarse spatial resolution data from multispectral sensors," *Int. J. Remote Sensing*, vol. 14, pp. 2231–2240, 1993.
- [32] Y. Kaufman and L. Remer, "Detection of forests using mid-IR reflectance: An application for aerosol studies," *IEEE Trans. Geosci. Remote Sensing*, vol. 32, pp. 672–683, May 1994.
- [33] B. Pinty and M. M. Verstraete, "GEMI: A nonlinear index to monitor global vegetation from satellites," *Vegetation*, vol. 101, pp. 15–20, 1992.
- [34] A. Dudhia, "Noise characteristics of the AVHRR infrared channels," *Int. J. Remote Sensing*, vol. 10, pp. 645–651, 1989.
- [35] A. W. Setzer and M. M. Verstraete, "Fire and glint in AVHRR's channel 3: A possible reason for the nonsaturation mystery," *Int. J. Remote Sensing*, vol. 15, pp. 711–718, 1994.
- [36] C. J. Tucker, "History of the use of AVHRR data for land applications," in *Advances in the Use of NOAA AVHRR Data for Land Applications*, G. D'Souza, A. S. Belward, and J. P. Malingreau, Eds. Dordrecht, The Netherlands: Kluwer, 1996, pp. 1–19.
- [37] J. R. G. Townshend, C. O. Justice, D. Skole, J. P. Malingreau, J. Cihlar, P. Teillet, F. Sadowski, and S. Ruttenberg, "The 1km resolution global data set: Needs of the International Geosphere Biosphere Programme," *Int. J. Remote Sensing*, vol. 15, pp. 3417–3441, 1994.
- [38] D. A. Griffith, "A spatially adjusted ANOVA model," *Geograph. Anal.*, vol. 10, pp. 296–301, 1978.
- [39] L. Anselin, "Spacestat tutorial: A workbook for using spacestat in the analysis of spatial data," Regional Res. Inst., West Virginia Univ., Morgantown, 1992.
- [40] R. W. Saunders, "The determination of broadband surface albedo from AVHRR visible and near-infrared radiances," *Int. J. Remote Sensing*, vol. 11, pp. 59–67, 1990.
- [41] P. J. Riggan, J. A. Brass, and R. N. Lockwood, "Assessing fire emissions from tropical savanna and forest of central Brazil," *Photogramm. Eng. Remote Sensing*, vol. 59, pp. 1009–1015, 1993.
- [42] J.-M. Grégoire, B. Glenat, E. Janodet, A. Tournier, P. A. Brivio, P. Barbosa, E. Barisano, S. Brownlee, P. Ceccato, H. Eva, P. Legeay-Janvier, D. Malibangar, J. M. Pereira, and M. J. Vasconcelos, "Satellite monitoring of vegetation fires for EXPRESSO, progress report no. II," Monitoring Tropical Vegetation Unit, Space Applicat. Inst., Joint Res. Centre, Ispra, Italy, Tech. Note 1.97.91, 1997.
- [43] L. R. Iversen, E. A. Cook, and R. L. Graham, "Regional forest cover estimation via remote sensing: The calibration center concept," *Landscape Ecol.*, vol. 9, pp. 159–174, 1994.
- [44] P. Mayaux and E. F. Lambin, "Estimation of tropical forest area from coarse spatial resolution data: A two-step correction function for proportional errors due to spatial aggregation," *Remote Sens. Environ.*, vol. 53, pp. 1–15, 1995.



José M. C. Pereira received the undergraduate degree in forestry in 1983 from the Instituto Superior de Agronomia, Universidade Técnica de Lisboa, Lisbon, Portugal, and the Ph.D. degree in renewable natural resources studies in 1989 from the University of Arizona, Tucson.

He is an Associate Professor with the Department of Forestry, Instituto Superior de Agronomia, Universidade Técnica de Lisboa, teaching courses in vegetation fires, forest ecology, and remote sensing.

His current research interests include the geographical ecology of wildfires in southern Europe and the development of remote-sensing algorithms for burned area mapping at regional and global scales.